AFOSR Scientific Report

AFOSR 69-2818TR

AN ENERGY APPROACH TO THE DYNAMIC STABILITY OF ARCHES

Maxwell C. Cheung and Charles D. Babcock, Jr.

Research Supported by

Air Force Office of Scientific Research

Office of Aerospace Research

United States Air Force

Grant AFOSR 68-1424

Graduate Aeronautical Laboratories

California Institute of Technology

Pasadena, California

September 1969

TABLE OF CONTENTS

AFOSR Scientific Report

AFOSR 69-2818TR

AN ENERGY APPROACH TO THE DYNAMIC STABILITY OF ARCHES

by

Maxwell C. Cheung and Charles D. Babcock, Jr.

Graduate Aeronautical Laboratories

California Institute of Technology

Pasadena, California

September 1969

TABLE OF CONTENTS

ACKNOWLEDGMENT

The authors wish to express their appreciation to Dr. E. E. Sechler for his advice. The support we received from Mr. George Carlson of the Aeronautics Shop and Mr. Marvin Jessey of the Electronics Laboratory is gratefully acknowledged. They also want to thank Miss Helen Burrus and Mrs. Betty Wood for preparing the manuscript.

This study was supported by the Air Force Office of Scientific Research, Office of Aerospace Research, United States Air Force under Grant No. AFOSR 68-1424.

ABSTRACT

Concentrated static and step loading were applied to circular arches with geometric parameters $7 < \gamma < 20$. The static equilibrium path and the dynamic response at the loading position were recorded. Dynamic buckling is distinct. Supercritical and subcritical response were separated by 0.5 per cent of the total load. The sensitivity of the arch to offset loading was studied. The effect was pronounced in the static tests but moderate in the dynamic case. An energy approach was used to determine the lower and upper bound for the critical step load. The lower bound agrees well with the experimental results.

NOMENCLATURE

A	Cross sectional area of the arch
b	Arch width
E	Young's Modulus
h	Arch thickness
H	Central arch rise
I	Moment of inertia
L	Arch length
ΔL	Distance between load and center of arch
N	Axial force
P	Concentrated load
$\overline{P}$	Nondimensional load $= \frac{PL^3}{16EI}\left(\frac{A}{I}\right)^{1/2}$
R	Arch radius
$S(t)$	Heaviside step function
t	Time
V	Potential energy of the system
$\overline{V}$	Nondimensional potential energy $= \frac{L^3A}{16EI^2} \cdot V$
w	Arch displacement
w_o	Initial arch shape $= H\left(1 - \frac{4x^2}{L^2}\right)$
x	Arch coordinate
$\overline{x}$	Nondimensional arch coordinate $= \frac{2x}{L}$
y	Nondimensional arch displacement $= \frac{w}{2}\sqrt{\frac{A}{I}}$
y_o	Nondimensional initial arch shape $= \frac{w_o}{2}\sqrt{\frac{A}{I}}$

NOMENCLATURE (cont'd)

β	Arch half angle
γ	Geometric parameter $= \frac{L^2}{4Rh}$
ϵ	Percentage of eccentricity $= \frac{\Delta L}{L}$
μ	Nondimensional axial strain
ρ	Mass density
τ	Nondimensional time $= \frac{4}{L^2}\sqrt{\frac{EI}{\rho A}} \cdot t$
$(\ )'$	$= \frac{\partial}{\partial \bar{x}}$
$(\dot{\ })$	$= \frac{\partial}{\partial \tau}$

Subscripts:

cr	Experimental critical value
cℓ	Classical theoretical value
max	Maximum value

I. INTRODUCTION

The stability of shell type structures under static loads has attracted much attention in the past few decades. The stability of the same type structures under dynamic loads is currently the subject of much investigation. However, considerable difficulties are encountered. First, the definition of dynamic stability is not as straightforward as in the static analysis. Secondly, the appropriate equations are now time dependent in addition to the spatial dependence of the static problem. The procedure most commonly used to solve these equations is to eliminate the spatial dependence by finite elements, finite difference, energy or Galerkin techniques and integrate the resulting time dependent equations numerically. The integration usually required exceedingly small time steps and convergence is a continual problem. In order to find the dynamic buckling load, the loading parameter must be incremented and the integration performed again until some type of critical load is found.

The establishment of a lower bound for the dynamic buckling load may prove to be a useful alternative to the above procedure. Analytical work along these lines has been carried out by several investigators (Refs. 1-5). In this method the knowledge of the static equilibrium positions for the structure is utilized to predict a lower bound on the dynamic buckling load under step or impulse loading. Unfortunately, the usefulness of the lower bound has not been demonstrated by comparison with experiments. The work reported in this paper is an effort to help fill part of this gap. Towards this purpose, the energy analysis and experiments have been carried out on a clamped

circular arch. The arch was chosen as a model structure because of its simplicity and the fact that it has many of the nonlinear characteristics of more complicated shell structures.

II. ANALYSIS

Using an energy type analysis, the dynamic stability of nonlinear elastic bodies subjected to step loading has been previously discussed by several authors. In order to clarify the concepts, the following discussion of a simple system is pursued.

First consider a nonlinear one degree-of-freedom system with a static load deflection curve of the form OABC as shown in Figure 1a. OA and BC represent stable branches while the AB branch is unstable under dead weight loading. Starting at the origin the maximum undamped dynamic response under a step loading is shown by the dotted line. The intersection of this curve with the branch AB is significant because this determines the load at which the undamped system will snap under step loading. This is easily seen by examining the potential energy curves for various load levels as shown in Figure 1b. Visualizing the system as a ball dropped from the origin of these curves, it is obvious that the deflection will be limited to a region near the origin as long as $P \leq P_D$. However if P is increased above P_D the ball (i.e. the nonlinear system) will cover additional territory. P_D is, therefore, defined as the critical dynamic load. The response histories at a supercritical and subcritical load level are illustrated at the left part of Figure 1a where time is plotted as the third axis perpendicular to the P-q_1 plane.

When a multi degree-of-freedom system is considered, the potential energy is no longer a single curve but a multi-dimensioned

manifold in a generalized coordinate space. In this case, the energy method fails to yield a unique critical condition. The alternative is to obtain the lower and upper bounds. The ideas can be adequately illustrated using a two degree-of-freedom model.

A typical static load deflection curve is shown in Figure 2a. The broken line OED is the q_1 component of the maximum dynamic response. The elliptic path between points A and B is the bifurcated branch. Therefore, there are always five equilibrium positions at the level $P_B < P < P_A$. These positions can be easily identified in the energy surfaces. Two such surfaces are illustrated in Figures 2b and 2c. The characteristics of the equilibrium positions are as follows: The center one is unstable (hill), the left and right ones are stable (depression), the upper and lower ones are unstable (saddle).

Figure 2b shows the constant load energy surface through D, the intersection of the dynamic and static deflection curve. At this load, the potential energy at the hill (center equilibrium position) is equaled to that at the origin. An infinitesimal increase of the load lowers the potential energy at the hill to below zero and allows the system to go over the large displacement region. Therefore this load level is the upper bound for the dynamic load.

The lower bound is shown in Figure 2c where the energy at the saddle points is zero. An infinitesimal decrease of the load causes the zero energy level contour to become multiconnected and the system does not have sufficient energy to go between the two regions.

The bounds discussed above are for elastic structures without damping. Should damping be present, the picture would be different. The lower bound is not affected because energy is needed to account for

dissipation. If the undamped system can not escape from the near stable region, the dissipative system also will not escape. However, the upper bound must be reconsidered. The amount of energy dissipated is a function of the dynamic path and thus depends on the initial conditions. An upper bound similar to the undamped case seems to be meaningless unless one can find a monotonically descending path on the energy surface that connects the origin to the far stable region. This is exactly the case for the static critical load where the saddle points merge with the near equilibrium position. Therefore, the static critical load is the upper bound for the damped system.

In order to calculate the upper and lower bounds on the dynamic buckling loads using the energy method, the static equilibrium positions must first be determined. For the shallow arch this can be accomplished in a straightforward manner as shown by Schreyer and Masur (Ref. 6). The analysis, including the potential energy of the arch, will be presented here for completeness.

A. Symmetric Equilibrium Positions

Using the coordinate system shown in Figure 3, the equation of motion of a shallow arch can be expressed in terms of the displacement as derived in reference 1.

$$EI\left(\frac{\partial^4 w}{\partial x^4} - \frac{\partial^4 w_o}{\partial x^4}\right) + N\frac{\partial^2 w}{\partial x^2} + \rho A\frac{\partial^2 w}{\partial t^2} + P\delta(x)S(t) = 0 \qquad (1)$$

where

$$N = \frac{AE}{2L}\int_{-L/2}^{L/2}\left[\left(\frac{\partial w_o}{\partial x}\right)^2 - \left(\frac{\partial w}{\partial x}\right)^2\right] dx$$

Substituting the nondimensional quantities,

$$y = \frac{w}{2}\cdot\sqrt{\frac{A}{I}} \qquad \tau = \frac{4}{L^2}\sqrt{\frac{EI}{\rho A}}\cdot t$$

$$y_o = \frac{w_o}{2}\cdot\sqrt{\frac{A}{I}} \qquad (\,)' = \frac{\partial}{\partial \bar{x}}$$

$$\bar{x} = \frac{2x}{L} \qquad (\dot{}\,) = \frac{\partial}{\partial \tau}$$

$$\bar{P} = \frac{PL^3}{16EI}\sqrt{\frac{A}{I}} \qquad \gamma = \frac{L^2}{4Rh}$$

Eq. (1) can be written in dimensionless form as follows,

$$y'''' + \mu^2 y'' + \ddot{y} + \bar{P}\,\partial(\bar{x})\,S(\tau) = 0 \tag{2}$$

where

$$\mu^2 = \int_{-1}^{1}\left[(y_o')^2 - (y')^2\right] dx \tag{3}$$

The corresponding static equation is

$$y'''' + \mu^2 y'' + \bar{P}\,\partial(\bar{x}) = 0 \tag{4}$$

The solution of (4) is

$$y_1 = A_1 \sin \mu\bar{x} + A_2 \cos \mu\bar{x} + A_3\bar{x} + A_4 \qquad [-1 \le \bar{x} < 0)$$

$$y_2 = B_1 \sin \mu\bar{x} + B_2 \cos \mu\bar{x} + B_3\bar{x} + B_4 \qquad (0 < \bar{x} \le 1] \tag{5}$$

The boundary conditions for a clamped arch are:

$$
\begin{aligned}
y_1(-1) &= 0 \\
y_1'(-1) &= y_o'(-1) = \sqrt{3}\gamma \\
y_2(1) &= 0 \\
y_2'(1) &= y_o'(1) = -\sqrt{3}\gamma
\end{aligned}
\tag{6}
$$

The continuity conditions and the jump in shear at the point of loading ($\bar{x} = 0$) are expressed as follows:

$$
\begin{aligned}
y_1(0) - y_2(0) &= 0 \\
y_1'(0) - y_2'(0) &= 0 \\
y_1''(0) - y_2''(0) &= 0 \\
y_1'''(0) - y_2'''(0) &= \bar{P}
\end{aligned}
\tag{7}
$$

Substitute (5) into (6) and (7), and provided that $\tan \mu \neq \mu$, the unknown constants are found as follows:

$$A_1 = -\frac{\bar{P}}{2\mu^3}$$

$$A_2 = \frac{1}{2\mu \sin\mu}\left[2\sqrt{3}\gamma + \frac{\bar{P}}{\mu^2}(\cos\mu - 1)\right]$$

$$A_3 = \frac{\bar{P}}{2\mu^2}$$

$$A_4 = \frac{\bar{P}}{2\mu^2}\left(1 - \frac{\sin\mu}{\mu}\right) - A_2\cos\mu$$

$$B_1 = \frac{\bar{P}}{2\mu^3}$$

$$B_2 = A_2$$

$$B_3 = -\frac{\bar{\bar{P}}}{2\mu^2}$$

$$B_4 = A_4$$

The constants $A_1, A_2, \ldots, B_4$ are functions of μ and $\bar{\bar{P}}$. The $\mu \sim \bar{\bar{P}}$ relationship can be found by substituting (5) into (3).

$$\mu^2 = 2\gamma^2 + (A_2^2 - A_1^2 + B_2^2 - B_1^2)\ \frac{\mu}{4} \sin 2\mu$$

$$- (A_1A_2 - B_1B_2)\ \mu \sin^2\mu - 2(A_1A_3 + B_1B_3) \sin \mu \qquad (9)$$

$$+ 2(A_2A_3 - B_2B_3)(\cos \mu - 1) - (A_1^2 + A_2^2 + B_1^2 + B_2^2)\ \frac{\bar{\bar{P}}^2}{2} - (A_3^2 + B_3^2)$$

The roots of this transcendental equation correspond to the value of μ at the equilibrium positions under the specified load level $\bar{\bar{P}}$.

B. Antisymmetric Equilibrium Positions

In evaluating (6), (7), the following algebraic equation must be solved

$$\begin{bmatrix} -\sin\mu & -1 \\ \mu\cos\mu & 1 \end{bmatrix} \begin{Bmatrix} A_1 \\ A_3 \end{Bmatrix} = \begin{Bmatrix} \frac{\bar{\bar{P}}}{2\mu^2}\left(\frac{\sin\mu}{\mu} - 1\right) \\ \frac{\bar{\bar{P}}}{2\mu^2}(1 - \cos\mu) \end{Bmatrix} \qquad (10)$$

If $\tan \mu = \mu$, A_1, A_3 can not be determined uniquely as in (8). The lowest possible μ that satisfies this condition is $\mu = 4.492$. In this case, only one of (10) is independent.

$$A_3 = \frac{\bar{P}}{2\mu^3}(\mu - \sin \mu) - A_1 \sin \mu \tag{11}$$

Substitute (11) and (5) into (3). A quadratic equation for A_1 is obtained.

$$\begin{aligned}&(\sin^2 \mu - \mu^2) A_1^2 + \frac{\bar{P}}{\mu^3}(\sin^2 \mu - \mu^2) A_1 \\ &+ \left[\mu(\sin \mu \cos \mu - \mu) A_2^2 + \frac{\bar{P}}{\mu^2}(\sin^2 \mu + 2 \cos \mu - 2) A_2\right. \\ &\left. + \frac{\bar{P}^2}{\mu^5}(\sin \mu - \mu) + 2\gamma^2 - \mu^2\right] = 0\end{aligned} \tag{12}$$

The A_2, A_4, B_1, B_2, B_3 and B_4 will be determined according to (8).

C. Potential Energy of the System

Let V designate the potential energy

$$V = \int_{-L/2}^{L/2} \frac{EI}{2}\left[\frac{\partial^2(w-w_o)}{\partial x^2}\right]^2 dx + \frac{1}{2} EAL\left(\frac{N}{AE}\right)^2 - P(w_o - w)\Big|_o \tag{13}$$

The nondimensional potential energy $\bar{V}$ is as follows:

$$\bar{V} = \int_{-1}^{1} (y'' - y_o'')^2 \, d\bar{x} + \frac{1}{2}\mu^4 - 2\bar{P}(y_o - y)\Big|_o \tag{14}$$

Substitute (5) into (14), we obtain

$$\overline{V} = \mu^3\left[\frac{\mu}{2}(A_1^2 + A_2^2 + B_1^2 + B_2^2) - \frac{1}{4}(A_1^2 - A_2^2 + B_1^2 - B_2^2)\sin 2\mu\right.$$

$$\left. - (A_1A_2 - B_1B_2)\sin^2\mu\right] + 2\sqrt{3}\gamma\mu\left[(A_1 - B_1)(1 - \cos\mu)\right. \qquad (15)$$

$$\left. - (A_2 + B_2)\sin\mu\right] + 6\gamma^2 + \frac{1}{2}\mu^4 - 2\overline{P}\left(\frac{\sqrt{3}}{2}\gamma - A_2 - A_4\right)$$

The results obtained above were evaluated numerically on an IBM 360/75 computer. The numerical results for the critical static load agree with the results obtained by Schreyer and Masur (Ref. 6). The values of the upper and lower bounds were numerically calculated and are compared with the experiment in Section IV.

III. EXPERIMENT

The arches used in the experiments were cut from 1/16 inch thick 2024-T3 aluminum sheet and were rolled to approximately 30 inch radius in a three roll roller. They were then heat treated for eight hours at 375 degrees Fahrenheit. The arches were mounted into a heavy steel frame for testing, the ends being secured using Devcon B. The geometry of the tested arches is listed in Table I.

There were three main steps in the complete testing of an arch. Namely, they were an initial imperfection measurement, a quasi-static test and a dynamic test. The arches were reusable and were reloaded at different locations, including from 0 °/o up to 6 °/o offset from the center. In between tests, imperfections of the arch

shape were measured in order to assure that the arch was not subjected to excessive plastic deformation.

A. Initial Imperfection Measurement

A pendulum like apparatus was built to measure imperfections of the arch. It consisted of a fixed center and rotatable arm which could be adjusted in length. A dial gauge was installed at the tip of the arm (see Figure 4).

The measurement was made by first adjusting the arm to the appropriate radius. Starting from one end of the arch the dial gauge readings were taken at half inch intervals along the arch. This measurement gave the deviation of the arch shape from the preset radius. Applying the "Least Square Method" to the measured data the "best fit radius" and the "best fit imperfection" can be found.

B. Static Tests

The static point load was applied using a knife edge. The knife edge was loaded through a stiff spring by a dead weight resting on a hydraulic jack. By slowly lowering the jack, the loading on the arch could be very smoothly increased. The load was measured using a strain gaged load link and the displacement of the knife edge was determined using a linear potentiometer. The load deflection curve was directly recorded on an XY plotter. A schematic of the loading device is shown in Figure 5.

C. Dynamic Tests

The dynamic step load was applied by preloading the knife edge that was used in the static tests but restraining the knife edge from

loading the arch with a pin. The pin was rapidly retracted transfering the load to the arch. The effect of the inertia of the weight was minimized by attaching it with a soft spring. With this arrangement, it was found that the variation in the load was less than 10 per cent of the total load. The large variation occurred after the arch buckled, thus its affect was small on the determination of the critical load. A Honeywell Visicorder (Model 1508) was used to record the displacement of the arch and the variation in the load. A photograph of the loading device is shown in Figure 6.

IV. TEST RESULTS

Four arches were used in the test program. These were selected to have the smallest imperfections. In addition, an effort was made to select arches with a minimum amount of nonsymmetric imperfection. The deviation from the best fit radius was less than 0.005 inches in all cases. The arches were used repeatedly until all information was acquired. Between tests, imperfections measurements show a slight plastic deformation around the point of loading. In spite of this, repeated tests showed almost identical response characteristics.

The critical static load and the effect of asymmetric loading is shown in Figure 7. In general, a 10 per cent reduction of critical load was detected when the load was applied offset from the center an amount equal to 6 per cent of the arch length. This effect was especially sensitive in the neighborhood of the center because the curve forms a cusp $\epsilon = 0$. Similar behavior was obtained theoretically and experimentally by Thompson for a truss structure (Ref. 7).

Figure 8 is a comparison of the experiments with the existing analysis. The critical loads are normalized by Schreyer and Masur's classical solution (Ref. 6). The upper curve is the classical solution for a sinusoidal arch (Refs. 2 and 3). The lowest curve is the static energy solution for clamped circular arches (Ref. 8). Experiments performed by Gjelsvik and Bodner are also shown on the figure.

It was observed on the load deflection diagram that the equilibrium paths crossed the abscissa (displacement axis) at no point other than the origin. Therefore, only the original configuration is a possible equilibrium position at the zero load condition.

A typical test result for the step loading experiment is shown in Figure 9. The figure shows the deflection-time traces at the loading point when a step load was applied.

The numbers attached to the curves are the loads expressed in pounds. The closest pair which change in nature defines the critical load. At the critical range, a one-half per cent change of load will result in a factor of three changes in response. The dotted straight lines represent the equilibrium position obtained from the static tests at the corresponding load levels. The subcritical responses were damped to the near equilibrium positions while the supercritical responses vibrated around the far equilibrium positions. If damping were not present, the supercritical response would have completed the bell shape curves as illustrated in Figure 1.

The effect of loading offset is shown in Figure 10. In contrast to static tests, the influence of the loading location is much less and the

reduction of the critical load appears to have a smooth transition near the center.

Finally, the dynamic critical loads were normalized by Schreyer and Masur's static classical solution, and are shown in Figure 11. In addition, the solution obtained by Vahidi (Ref. 5) using finite differences and direct numerical integration of the equations is shown in the figure. For these experiments the agreement with either of the two analysis is good.

V. CONCLUSIONS

Overall, the static tests agree reasonably well with Schreyer and Masur's solution. The somewhat lower results are probably caused by initial imperfections. The results are sensitive to the position of the loading as shown in Figure 7.

The step loading tests showed a very distinct dynamic buckling phenomenon. The critical load was determined to within 1/2 per cent for all cases. The influence of a load offset was not as important as in the static case.

As shown in Figure 11, the agreement between the dynamic critical load and the lower bound was found to be good. The bound shown in the figure is virtually the same if calculated using the saddle point or the unstable symmetric position. This is due to the fact that the asymmetric deflection is not decisive in this problem since it bifurcates, not from the stable side of the load deflection curve, but from the unstable side. This has previously been pointed out in reference 6.

The reason why the lower bound is above the critical load obtained by Vahidi, who used numerical integration is not clear. However, the difference between the results from the two analyses is very small. The experiments are also slightly below the lower bound. While this is somewhat disconcerting, the difference could again be explained by initial imperfections as in the static case. Despite this small inconsistency, the usefulness of the energy method for this simple structure has been demonstrated. This encourages an extension of this type of analysis to more complicated structures where a direct solution of the differential equations is impractical.

Finally, it was found that the original rest configuration of the arch was the only equilibrium position at the zero load condition. This is in agreement with Vahidi's calculation (Ref. 9). Since the existence of other equilibrium positions is a requirement in an energy approach to determine the critical load level, the impulsive loaded clamped circular arch can not be rigorously classified as a dynamic buckling problem.

REFERENCES

1. Hoff, N. J. and Bruce, V. G., "Dynamic Analysis of the Buckling of Laterally Loaded Flat Arches", J. Math. Phys., 32, pp. 276-288, (1954).
2. Simitses, G. J., "Dynamic Snap-Through Buckling of Low Arches and Shallow Spherical Caps", Ph. D. Dissertation, Dept. of Aeronautics and Astronautic, Stanford University, (June 1965).
3. Hsu, C. S., "Equilibrium Configurations of a Shallow Arch of Arbitrary Shape and Their Dynamic Stability Character", Int. J. Non-Linear Mech., 3, pp. 113-136, (1968).
4. Cheung, M. C., "The Static and Dynamic Stability of Clamped Shallow Circular Arches", Ph. D. Dissertation, Department of Aeronautics, California Institute of Technology, (1969).
5. Vahidi, B., "Some Aspects of Dynamic Snap-Through Problems", Ph. D. Dissertation, Department of Applied Mechanics, University of California, San Diego, (1969).
6. Schreyer, H. L. and Masur, E. F., "Buckling of Shallow Arches", J. Eng. Mech. Div., Proc. ASCE, pp. 1-17, (August 1966).
7. Thompson, J. M. T., "Dynamic Buckling under Step Loading", Dynamic Stability of Structures, Edited by Herrmann, G., Pergamon Press, pp. 215-236, (1967).
8. Gjelsvik, A. and Bodner, S. R., "The Energy Criterion and Snap Buckling of Arches", J. Eng. Mech. Div., ASCE, pp. 87-134, (Oct. 1962).
9. Vahidi, B., "Non-Existence of Snap-Through for Clamped Shallow Elastic Arches Subjected to Impulsive Load", TR No. 8, University of California, San Diego, (March 1968).

TABLE I

Geometric Descriptions of the Tested Arches

	Arch 1	Arch 2	Arch 3	Arch 4
b (in)	0.75	0.75	0.75	0.75
h (in)	0.0632	0.0643	0.0643	0.0643
L (in)	12.20	10.90	9.50	7.75
R (in)	31.56	32.09	32.01	31.58
*γ	18.655	14.395	10.962	7.395
*H (in)	0.5895	0.4628	0.3524	0.2377
*β (degree)	11.075	9.729	8.503	7.030

* Calculated

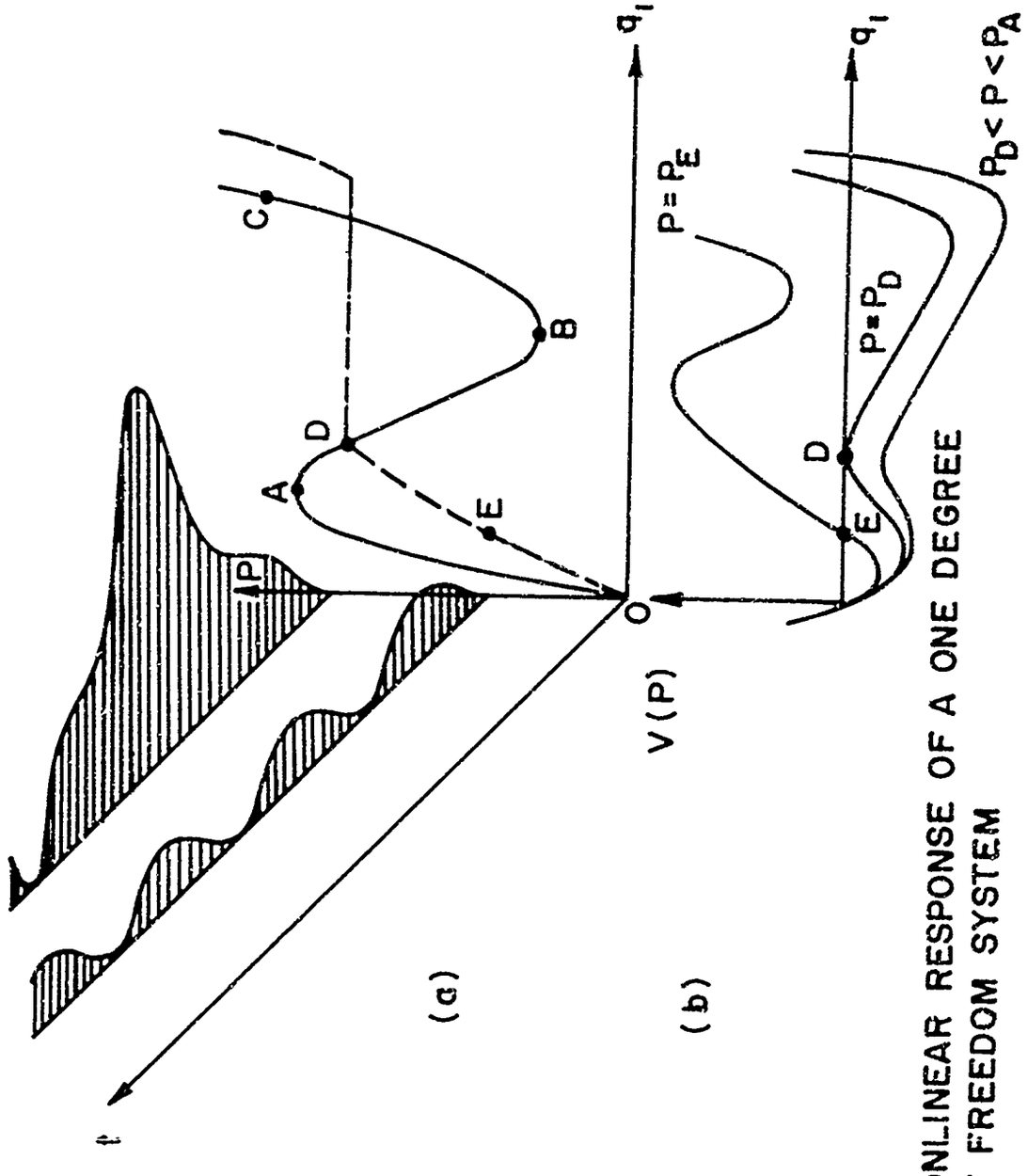

FIG. 1 NONLINEAR RESPONSE OF A ONE DEGREE OF FREEDOM SYSTEM

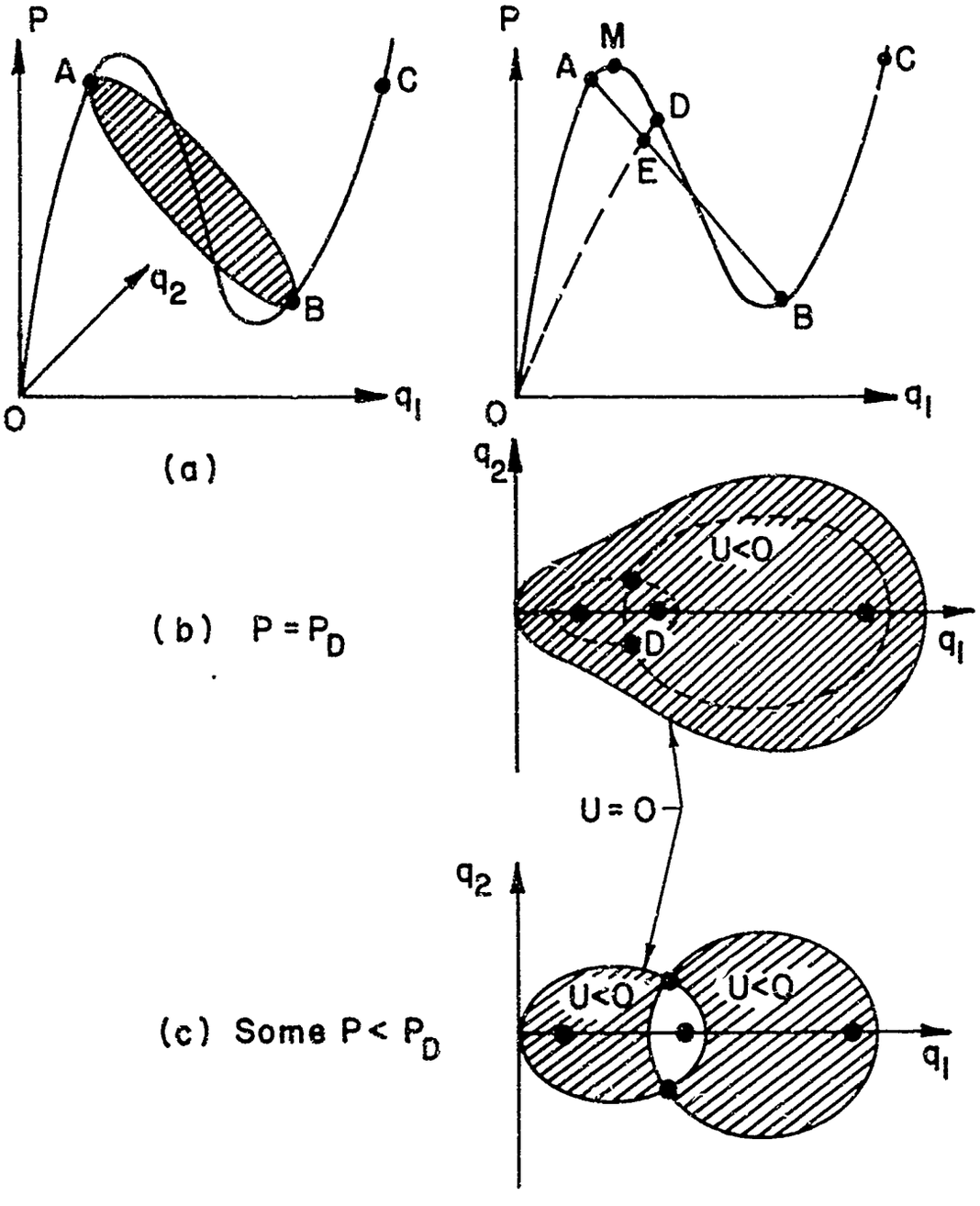

FIG. 2 NONLINEAR RESPONSE OF A TWO DEGREE OF FREEDOM SYSTEM

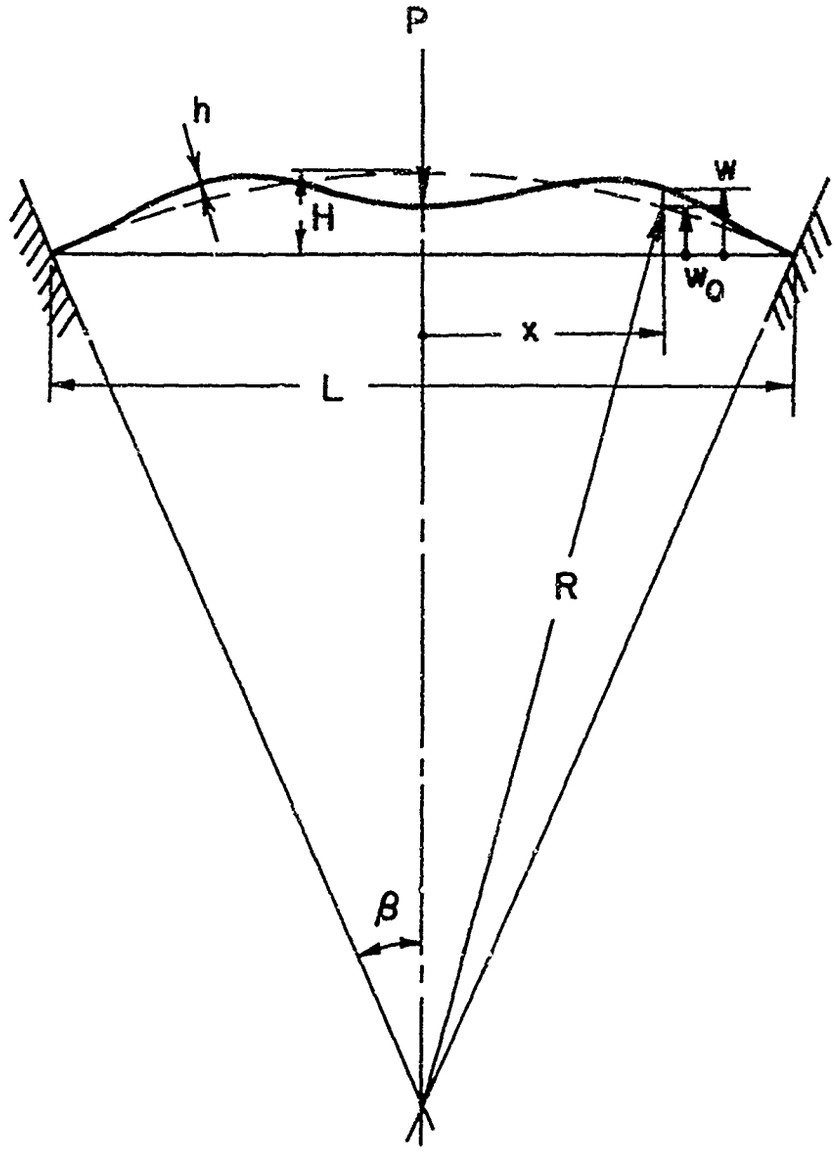

FIG. 3 COORDINATE SYSTEM FOR THE CLAMPED CIRCULAR ARCH

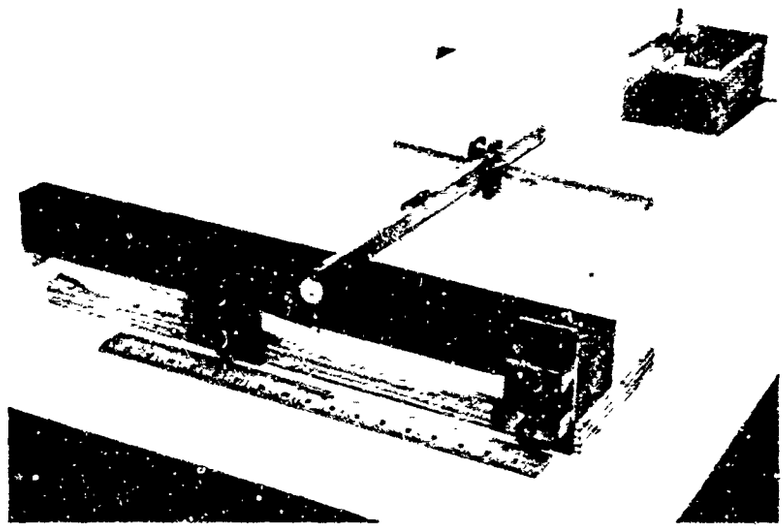

Fig. 4. Measuring of Initial Imperfection of a Circular Arch.

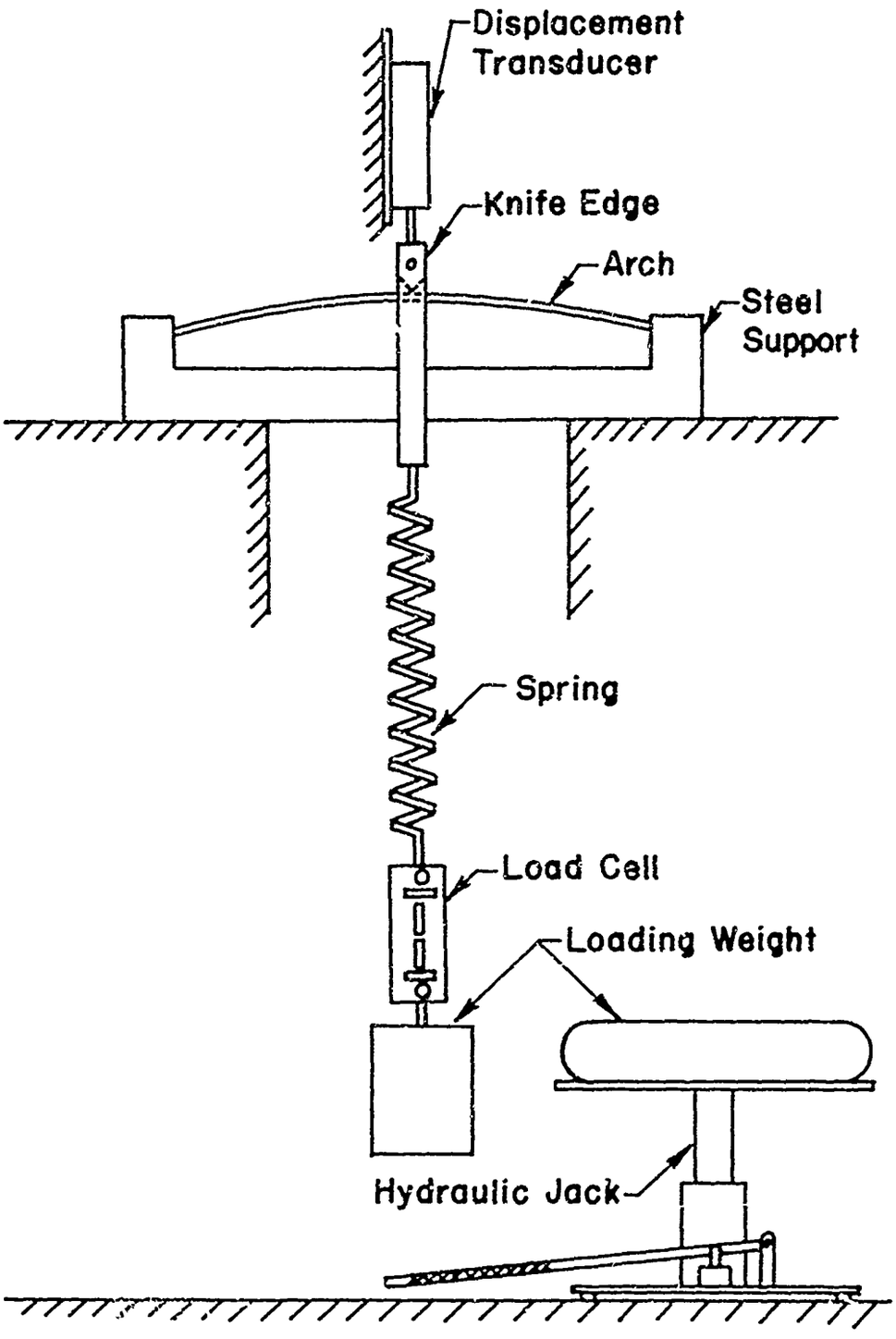

FIG. 5 THE STATIC AND DYNAMIC TEST APPARATUS

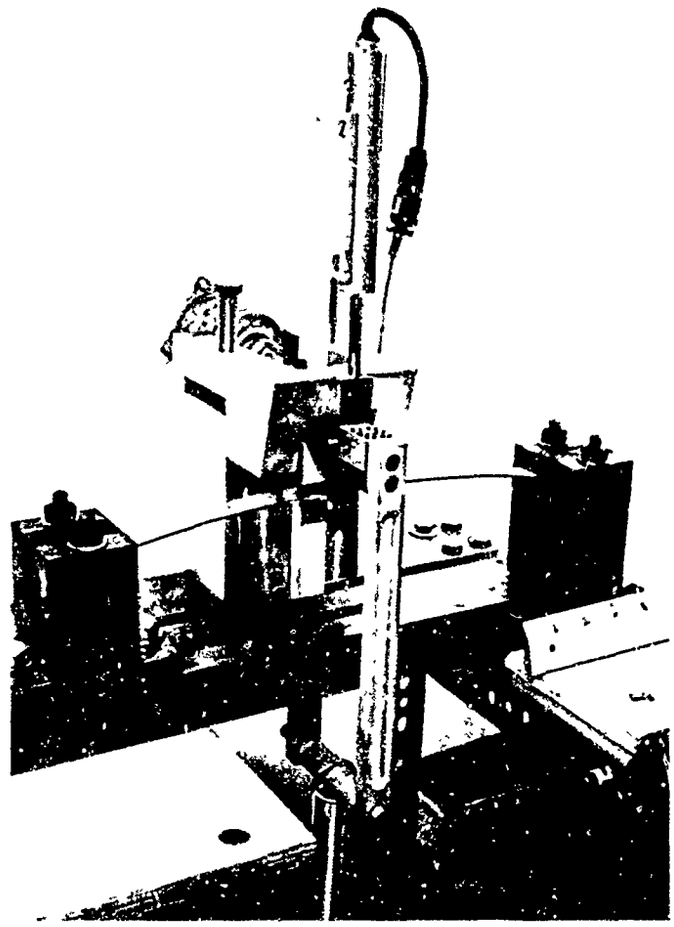

Fig. 6. Knife Edge Assembly.

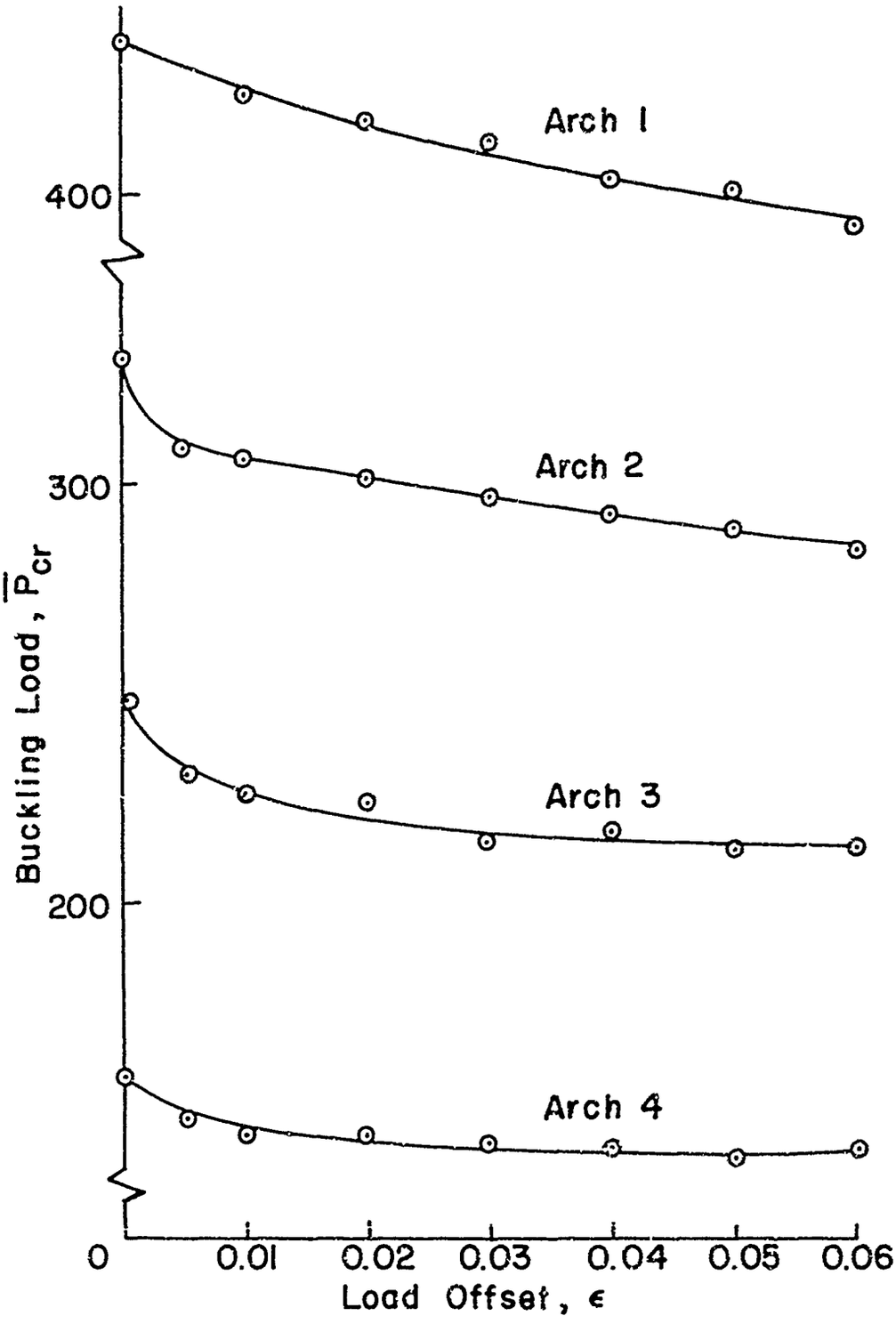

FIG. 7 NONDIMENSIONAL CRITICAL STATIC LOAD VS. LOAD OFFSET

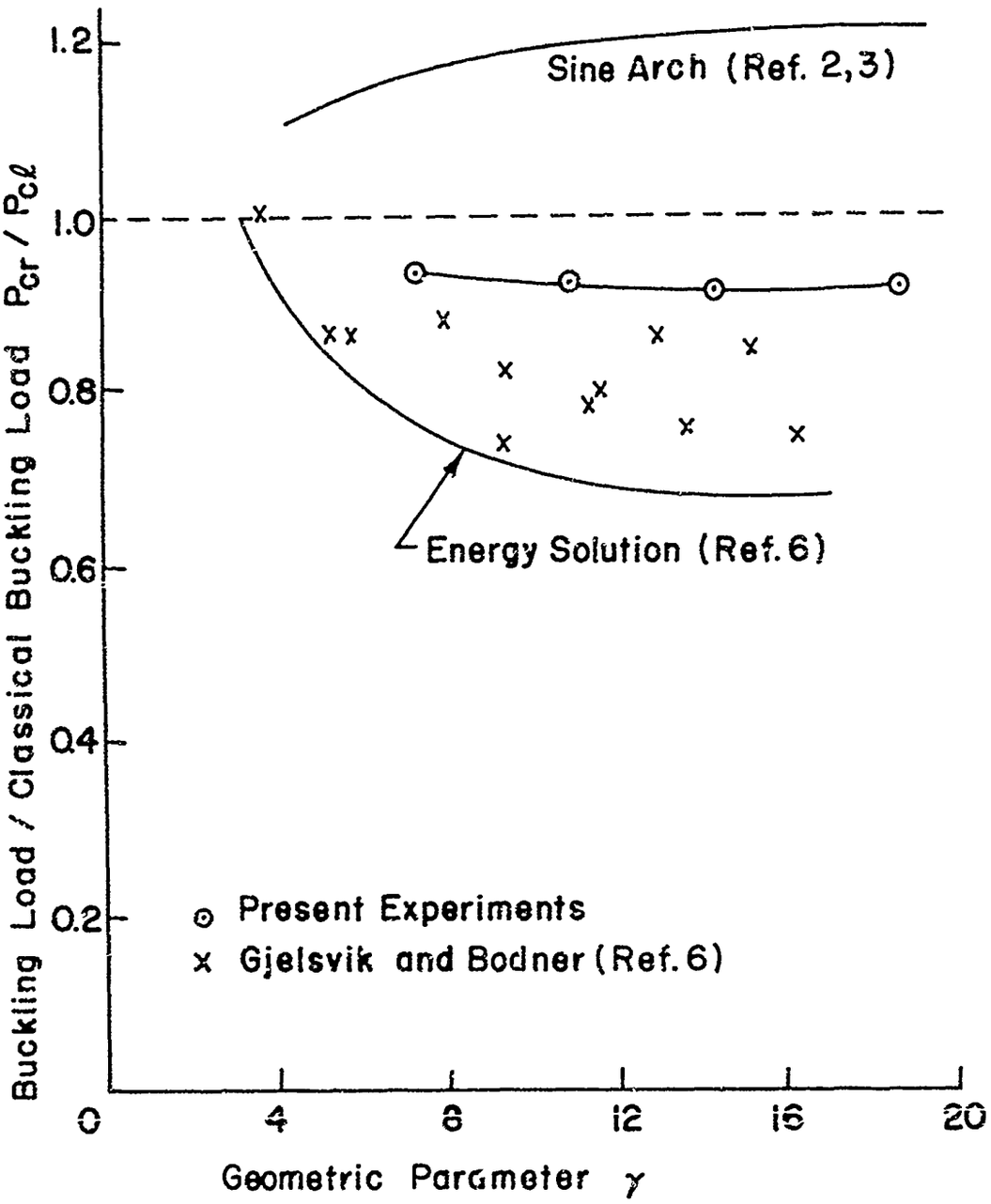

FIG. 8 COMPARISON OF STATIC EXPERIMENTS TO THE THEORETICAL STATIC BUCKLING LOAD

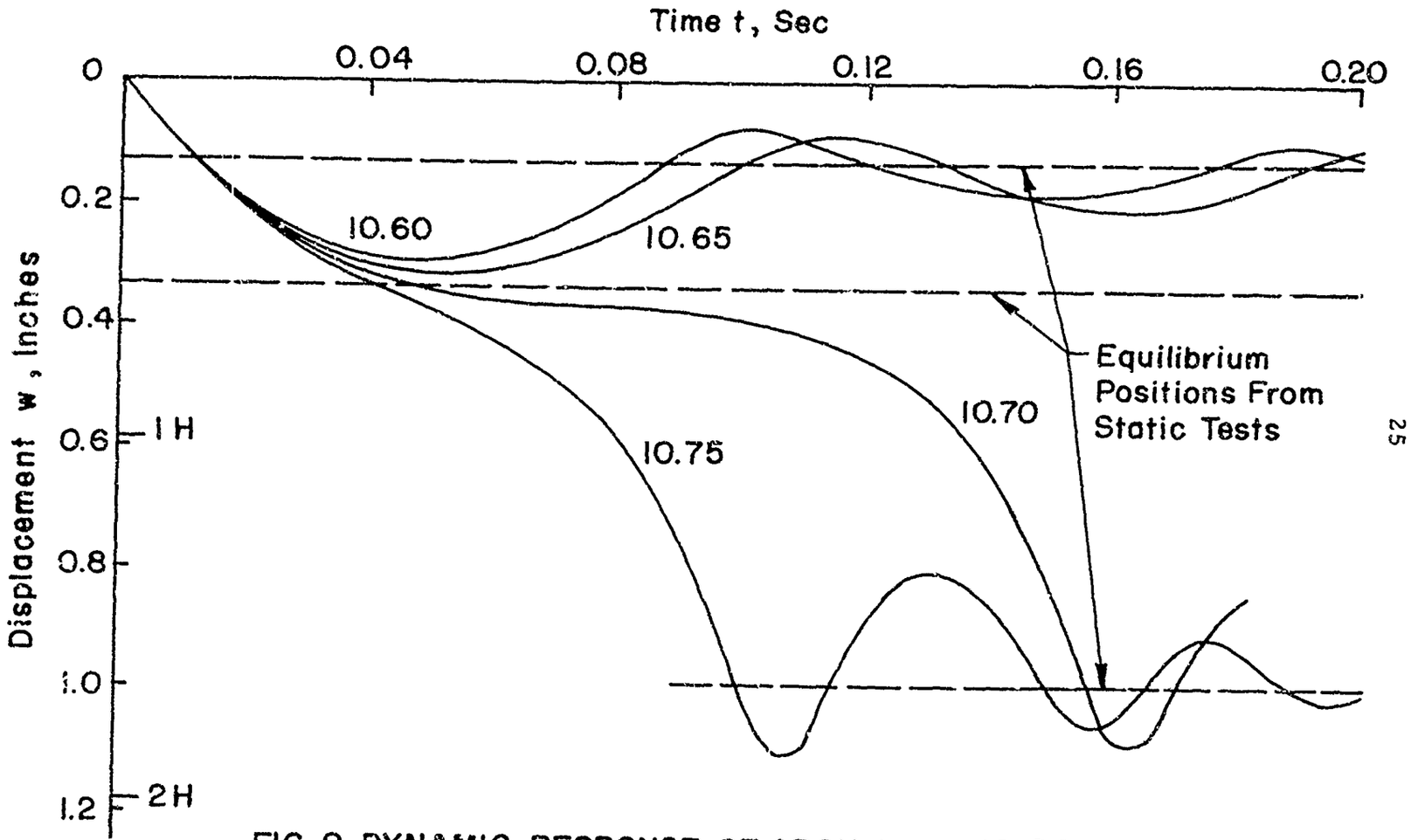

FIG. 9 DYNAMIC RESPONSE OF ARCH 1, $\gamma = 18.66$, $\epsilon = 0$

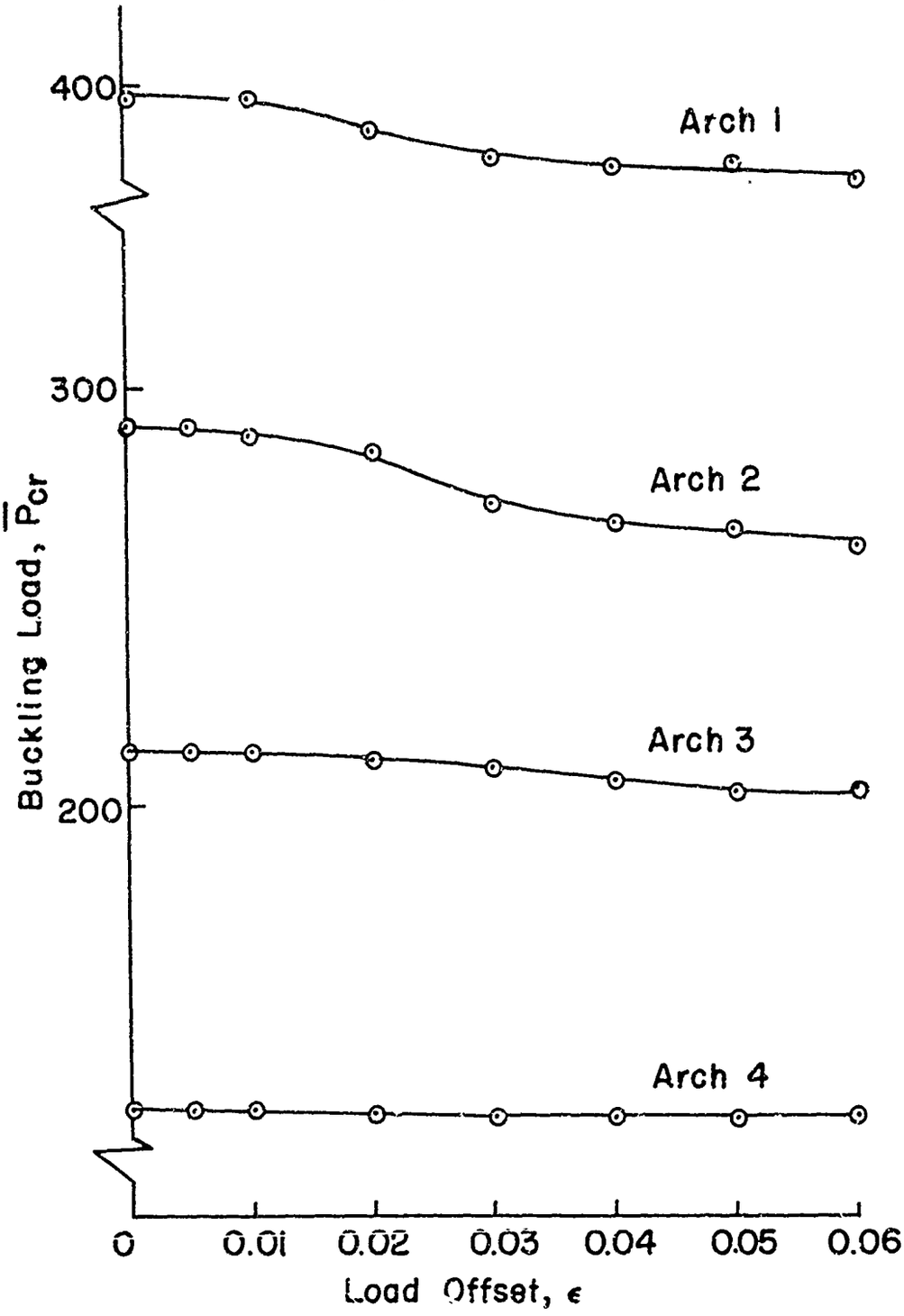

FIG. 10 NONDIMENSIONAL CRITICAL STEP LOAD VS. LOAD OFFSET

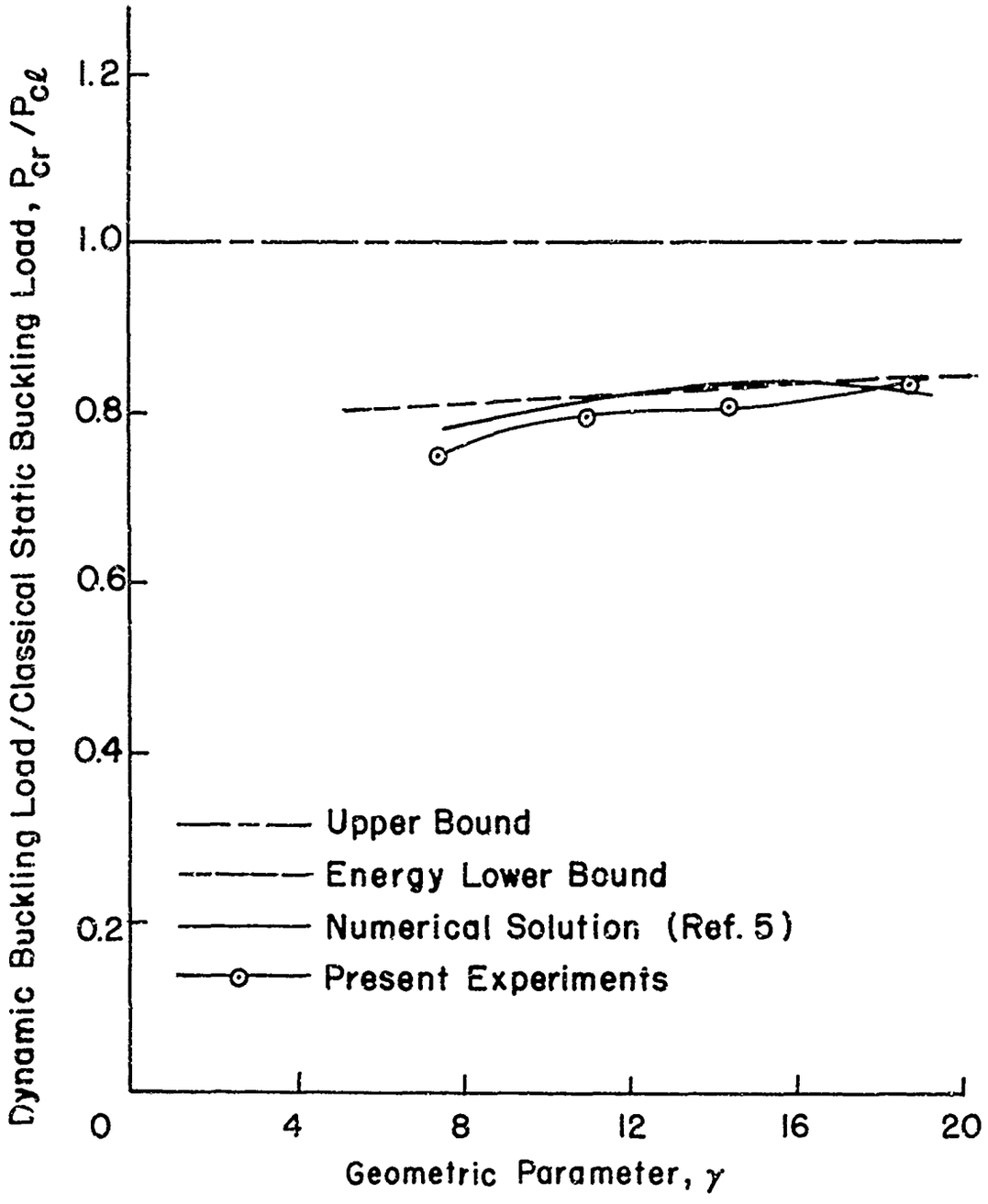

FIG. 11 COMPARISON OF DYNAMIC EXPERIMENTS TO THE THEORETICAL STEP BUCKLING LOAD

Security Classification

DOCUMENT CONTROL DATA - R & D

Security classification of title, body of abstract and indexing annotation must be entered when the overall report is classified)

1. ORIGINATING ACTIVITY (Corporate author) Graduate Aeronautical Laboratory California Institute of Technology Pasadena, California 91109	2a. REPORT SECURITY CLASSIFICATION UNCLASSIFIED 2b GROUP

3. REPORT TITLE

AN ENERGY APPROACH TO THE DYNAMIC STABILITY OF ARCHES

4. DESCRIPTIVE NOTES (Type of report and inclusive dates)

Scientific Interim

5. AUTHOR(S) (First name, middle initial, last name)

Maxwell C. Cheung and Charles D. Babcock Jr

6. REPORT DATE	7a. TOTAL NO OF PAGES	7b. NO OF REFS
September 1969	33	9

8a. CONTRACT OR GRANT NO	9a. ORIGINATOR'S REPORT NUMBER(S)
AFOSR -1424	
b. PROJECT NO 9782-01 61102F d 681307	SM 69-11 9b OTHER REPORT NO(S) (Any other numbers that may be assigned this report) AFOSR 69-2818TR

10. DISTRIBUTION STATEMENT

1. This document has been approved for public release and sale; its distribution is unlimited.

11. SUPPLEMENTARY NOTES	12. SPONSORING MILITARY ACTIVITY
TECH, OTHER	AF Office of Scientific Research (SREM) 1400 Wilson Boulevard Arlington, Virginia 22209

13. ABSTRACT

Concentrated static and step loading were applied to circular arches with geometric parameters $? < \gamma < 20$. The static equilibrium path and the dynamic response at the loading position were recorded. Dynamic buckling is distinct. Supercritical and subcritical response were separated by 0.5 per cent of the total load. The sensitivity of the arch to offset loading was studied. The effect was pronounced in the static tests but moderate in the dynamic case. An energy approach was used to determine the lower and upper bound for the critical step load. The lower bound agrees well with the experimental results.

DD FORM 1473

UNCLASSIFIED
Security Classification

14 KEY WORDS	LINK A		LINK B		LINK C	
	ROLE	WT	ROLE	WT	ROLE	WT
Dynamic Buckling						
Clamped Arches						
Step Load						